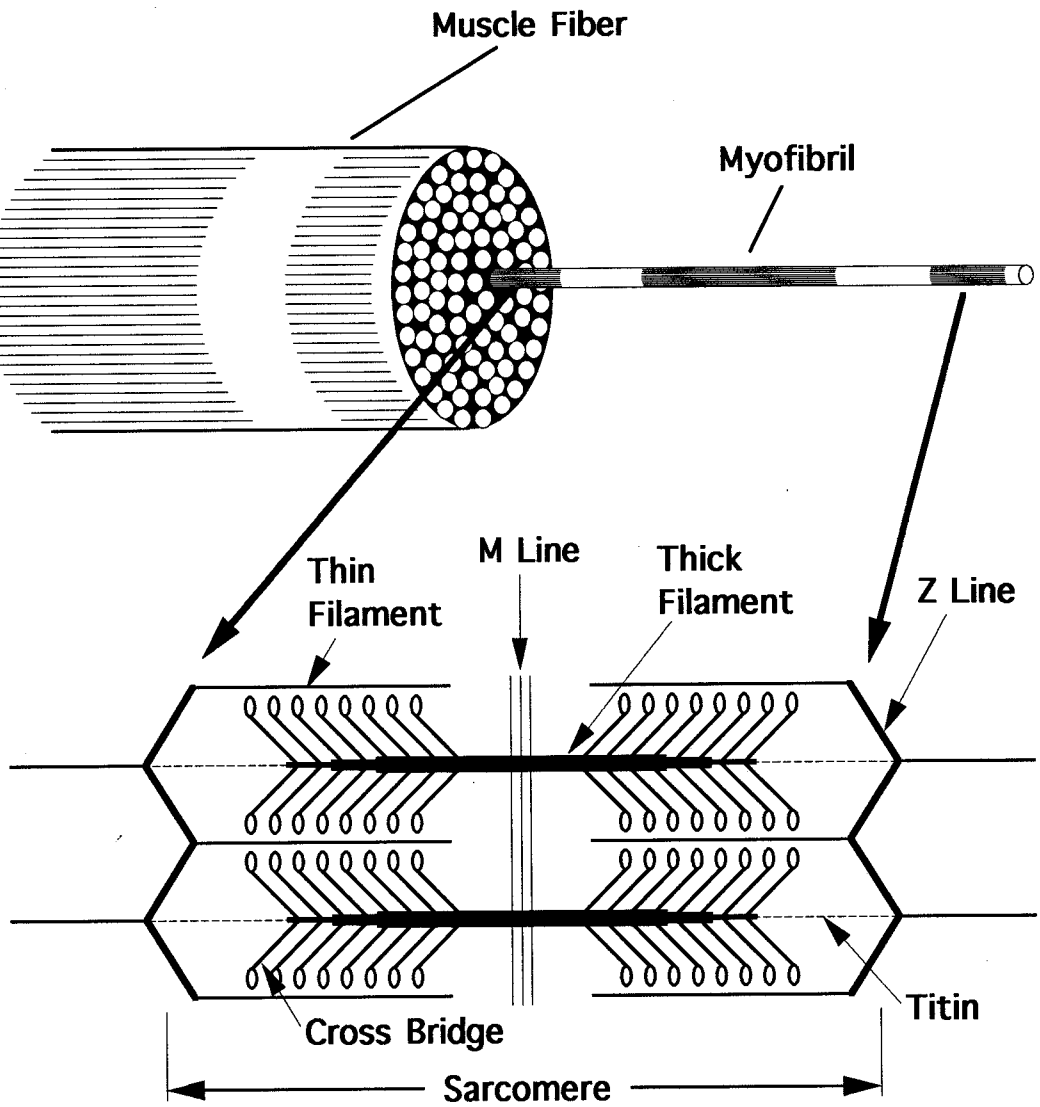

Figure 1.1. Structure of muscle tissue showing the arrangement of muscle fibers, myofibrils, and sarcomeres within muscle tissue. The sarcomere is the fundamental contractile unit of muscle. Each titin molecule spans from the Z line to the M line, thus covering one half of the length of the sarcomere. From the M line to each end of the thick filament, the titin molecule is mechanically associated with the thick filament and is thought to be relatively inextensible. Between the end of the thick filament and the Z line, the titin molecule contains a unique and recently discovered structural motif, known as the PEVK sequence (Labeit and Kolmerer, 1995), which is thought to contribute significantly to the spring-like extensibiltiy of the titin molecule.

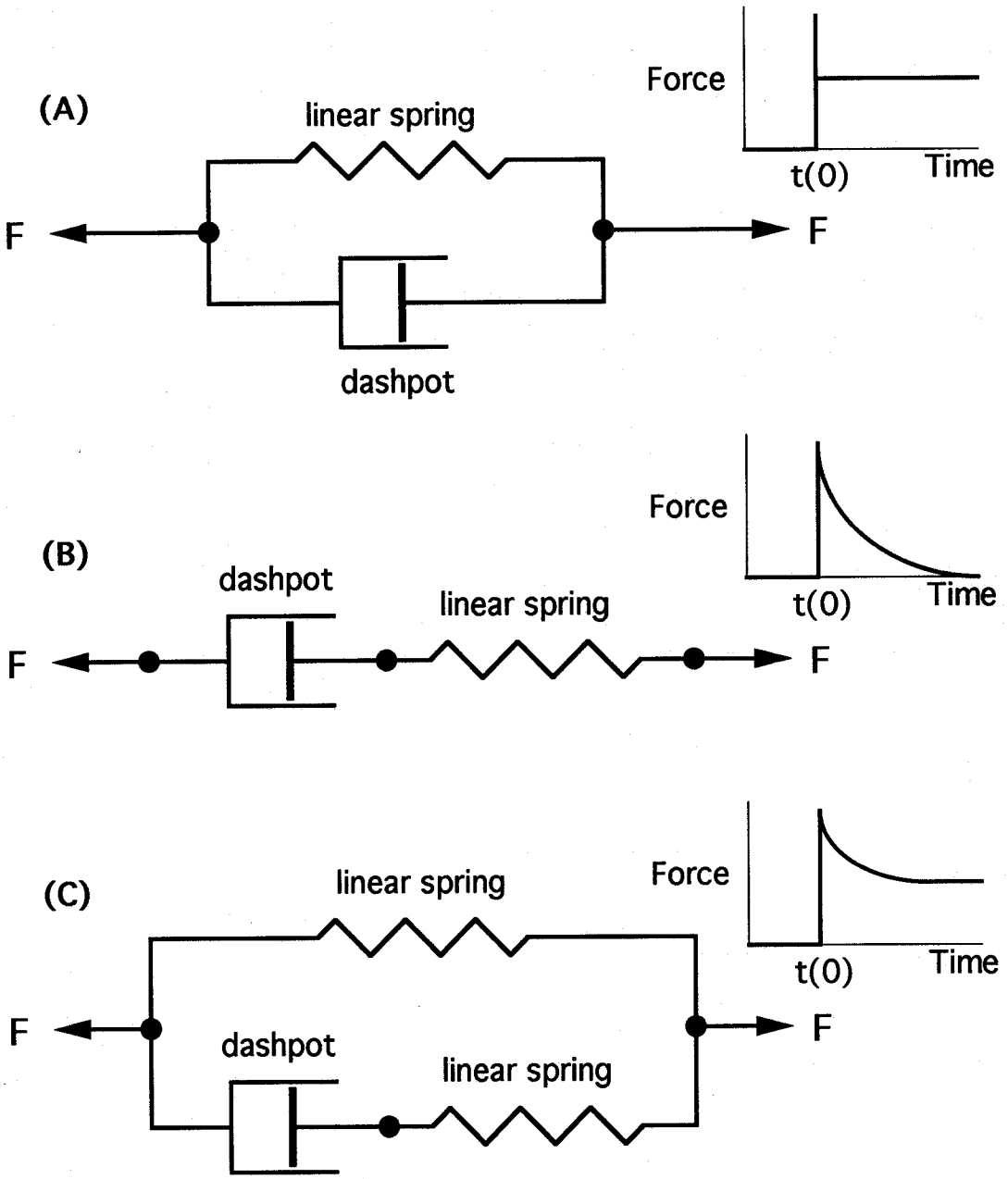

Figure 1.2. Standard models of viscoelasticity: (A) the Voight model, (B) the Maxwell model, and (C) the Standard Linear Solid, or Kelvin model. Each of the models assumes linear springs and dashpots. The relaxation function for each of the models is shown above and to the right of each model. The relaxation function is generated by subjecting the viscous body to a step length increase at time t(0). The models assume instantaneous length increase as well as uniform longitudinal strain in the physical samples that are modeled. Note that in each case the resulting force is reduced after the application of the step. These models are used to characterize the viscoelasticity of biological tissues (Fung, 1993).

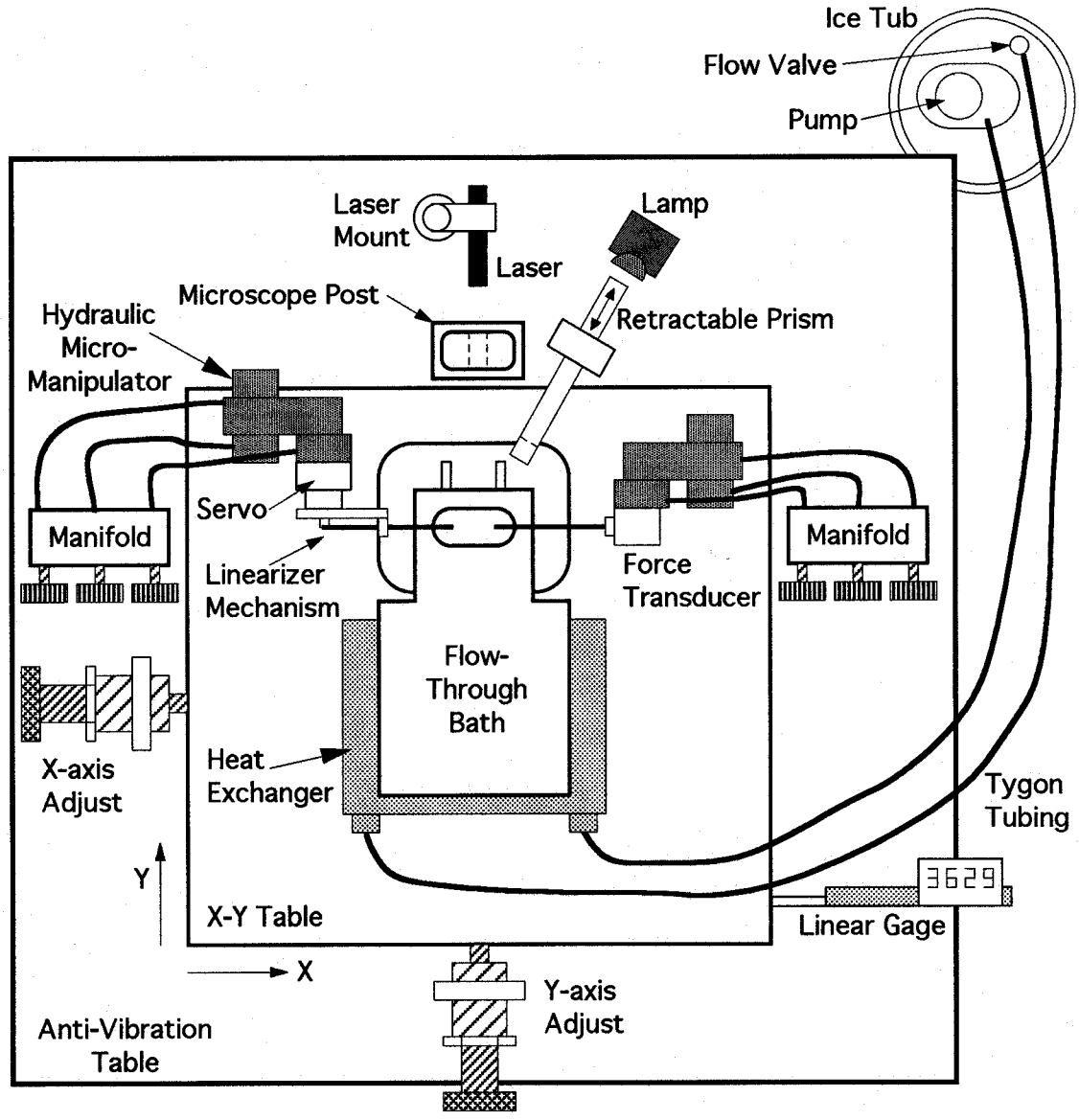

Figure 2.1. Mechanical schematic of the experimental setup. The stereo microscope (not shown) is mounted to the microscope post and sits directly above the flow-through bath. The muscle fiber is mounted into the flow-through bath (Fig 2.3) which is bolted to the X-Y table, which in turn is bolted to an anti-vibration table. The X-Y table position is adjusted by a pair of triple nested-thread actuators, allowing coarse and very fine movements in the X and Y directions. The X-Y table movement in the X direction is measured using a digital linear gage made from a digital caliper. The table can be positioned in the X direction to the nearest 0.01mm. The servo and force transducer are also mounted to the X-Y table on independent, 3-axis hydraulic micromanipulators. Each micromanipulator is controlled manually by a master cylinder manifold. The detector array is mounted below the antivibration table and is not shown in this schematic. The flow-through bath temperature is maintained by controlling the flow of ice water through a heat exchanger. The laser is mounted to the anti-vibration table with an adjustable mechanism for alignment. The laser beam passes through a slot in the microscope mount, and is then focused and reflected down to strike the muscle fiber (Fig 2.1).

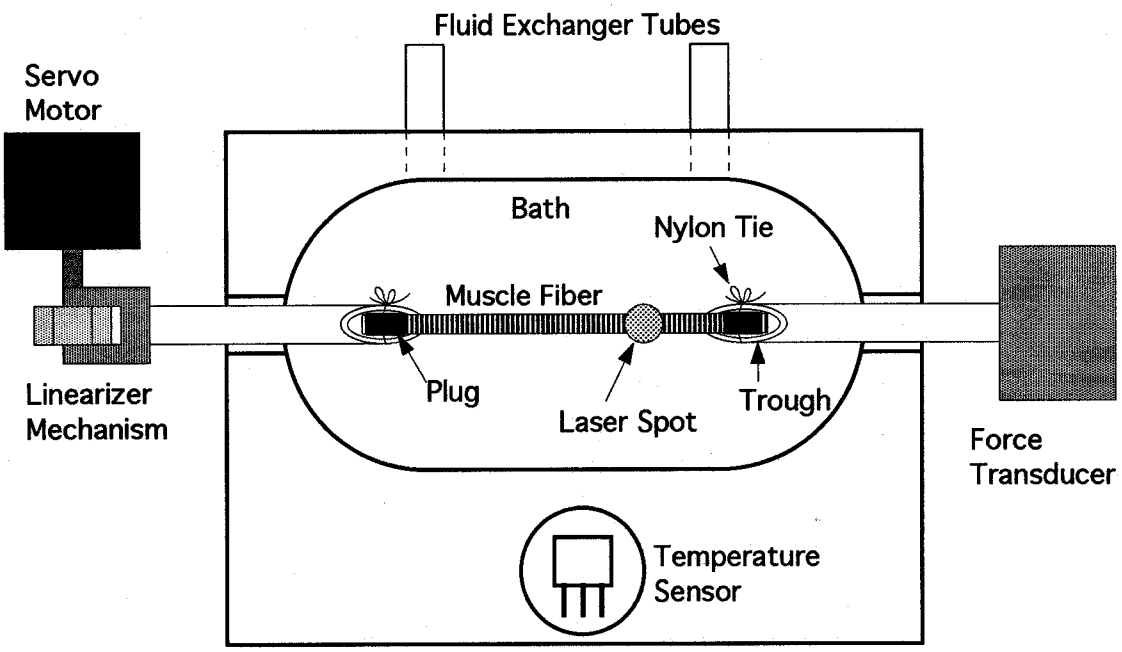

Figure 2.2. Top view of the muscle fiber mounted in the experimental apparatus. This is very similar to the view when the stereo misroscope is at low magnification with the dissecting objective in place. The fiber is mounted to stainless steel troughs made from 29 gage thin-wall stainless tubing. The troughs are formed by filing a 0.9 mm long segment at the end of each piece of sainless steel tubing to half the thickness of the original tube. The bath is filled with relaxing fluid prior to mounting the fiber. The ends of the fiber are placed into the troughs as shown, and are held in place by 0.6 mm long plugs made from 5-0 nylon monofilament suture. The plugs are tied to the troughs by a single strand of waxed dental floss. The use of two ties per plug reduces the tendency of the fiber to slip out from under the plug. The position of both the force transducer and the servo motor can be independently controlled on three axes. This allows the fiber to be positioned in the center of the bath, level, and such that the servo trough axis, the muscle fiber, and the force transducer trough are all coaxial. The servo motor is then translated left or right to adjust the sarcomere length of the muscle fiber. The laser spot is clearly visible on the fiber when the laser is turned on and the prism (Fig. 2.1) is slid into place, and the entire assembly shown above can be translated left or right on the X-Y table to place the laser spot at any desired position on the fiber.

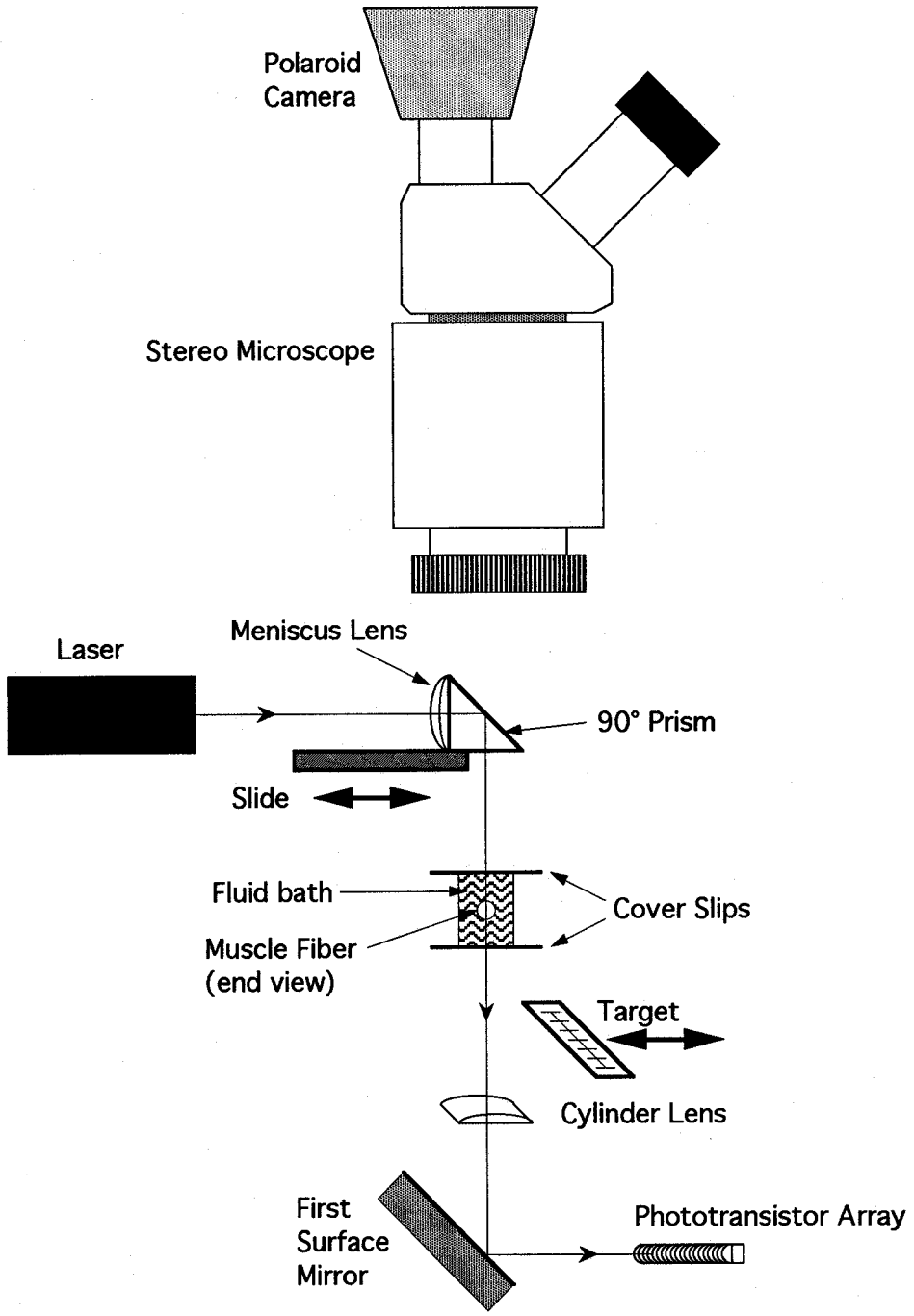

Figure 2.3. Schematic diagram of the optical elements in the experimental setup. The muscle fiber is suspended in a fluid bath as shown. During setup, the meniscus lens and prism are retracted to allow viewing of the fiber by means of the stereo microscope. After the muscle fiber is in place and the top cover slip has been added, the laser is turned on and the meniscus lens and prism are slid into position as shown. A small target is placed in the optical path below the fiber to allow the diffraction pattern to be read directly during sarcomere length adjustment. During the pulse propagation experiments, the diffraction pattern is projected onto the phototransistor array. The diffraction pattern is focused by the cylinder lens to maximize the signal strength on the sensitive area of the phototransistor array.

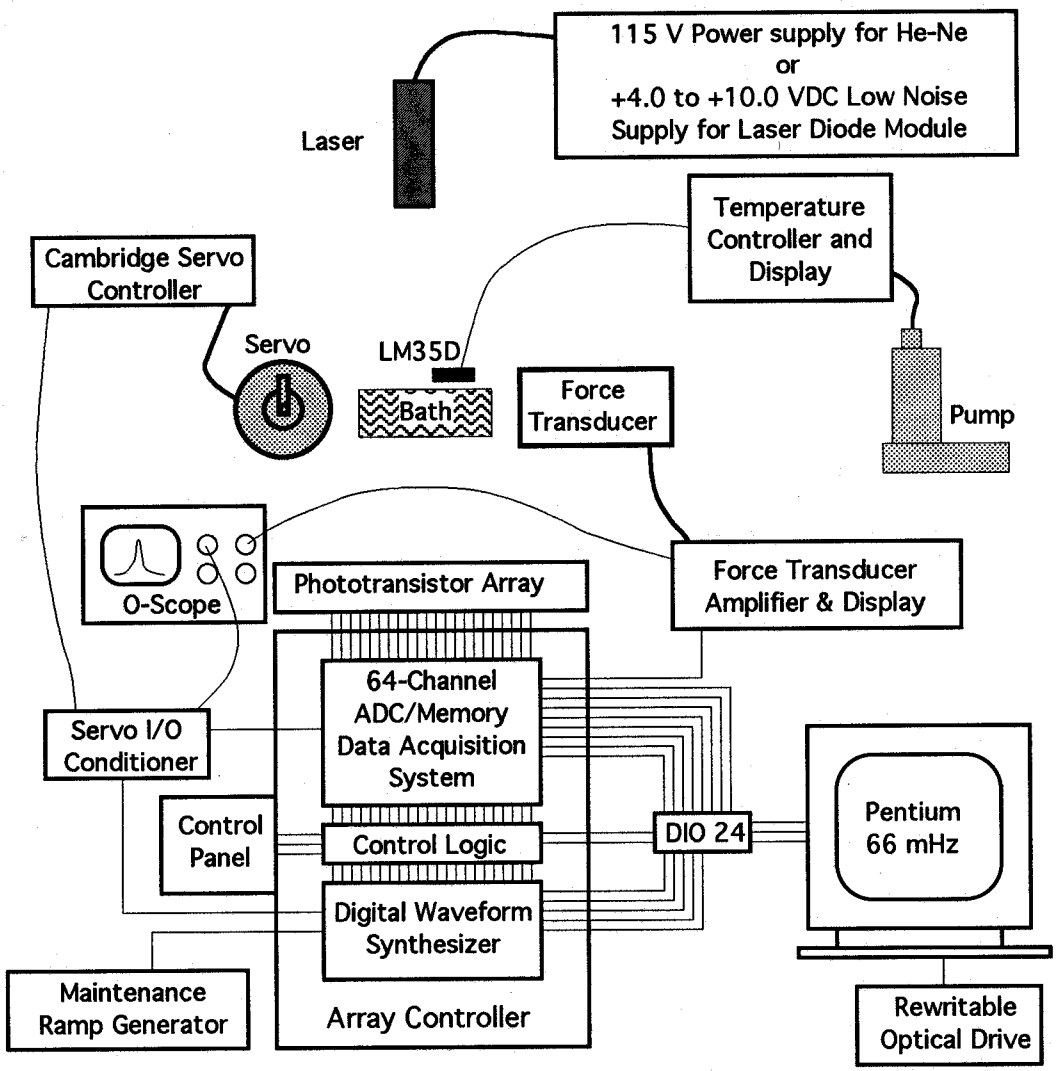

Figure 2.4. Schematic of the total electrical system of the experimental setup. The array controller is a large integrated system which includes the phototransistor array, a 64-channel parallel data acquisition system, a four channel parallel digital waveform synthesizer, a control panel, and control logic to integrate the system. The experimental sequence is loaded from the computer into the digital waveform synthesizer. The computer interfaces with the array controller system via a standard 24-bit digital I/O card (National Instruments DIO-24). After the muscle fiber is placed in the setup, the experiment is executed either from the control panel on the array controller or remotely from the computer. During execution of the experiment, the digital waveform synthesizer generates control signals for the servo motor. These are conditioned by the servo I/O conditioner to maximize the servo performance. A maintenance ramp signal is also available to provide shortening ramps for muscle fiber maintenance, as described in the text. Muscle fiber force is detected by an optical force transducer, the output of which is amplified and displayed digitally to the nearest 1 μN. Servo position and muscle fiber force are displayed on an oscilloscope during the experiment, and are recorded by the array controller system. Bath temperature is controlled and displayed as described in the text. When the experimental sequence is complete, the data are downloaded from the memory in the 64-channel data acquisition system to the computer via the DIO 24 interface.

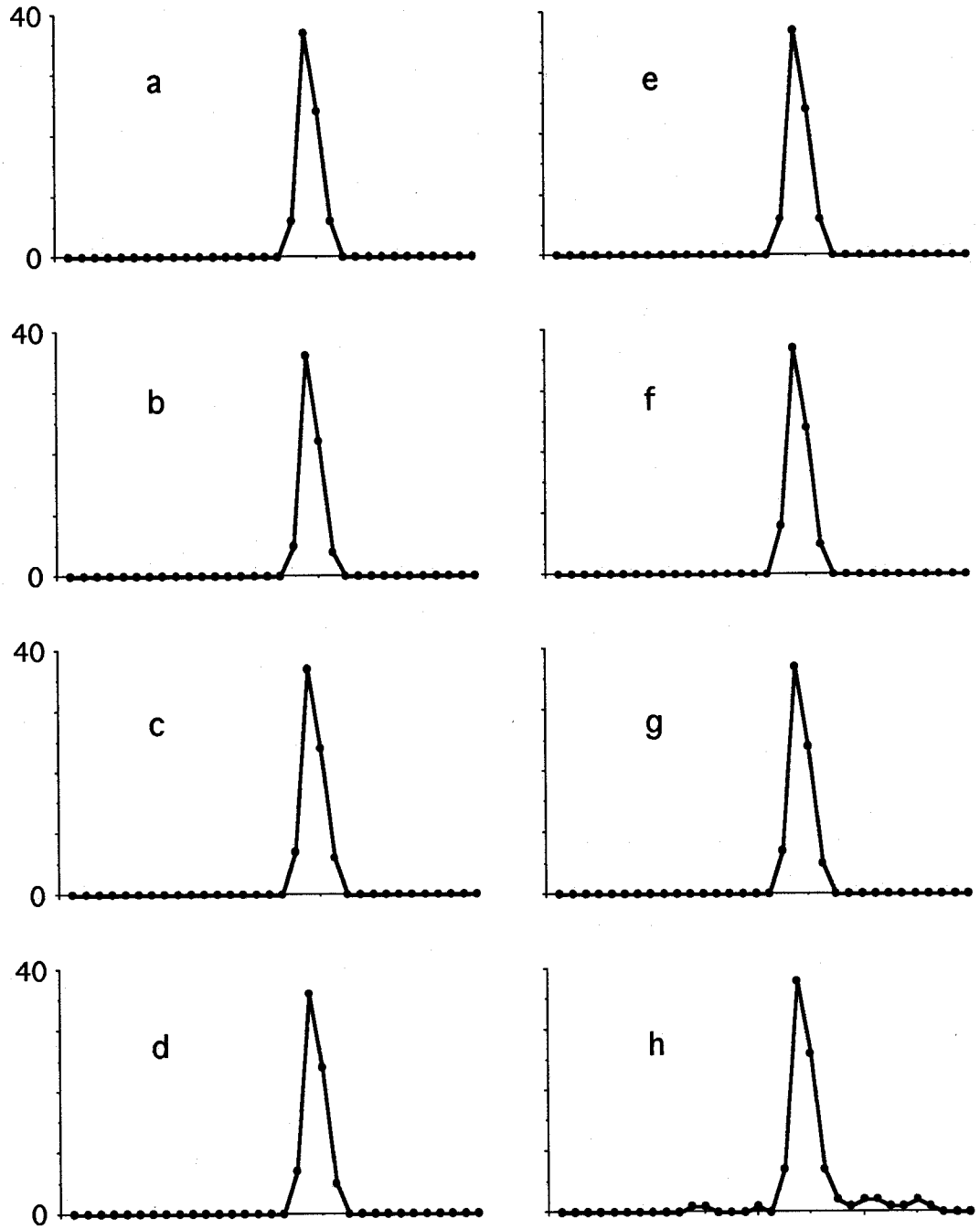

Figure 2.5. A series of eight consecutive diffraction spectra from Fiber 19, indicated as letters **a** through **h**. The data were collected from one of the first order diffraction peaks (right side as viewed on the apparatus). The light source was a 10 mW He-Ne laser (632.8 nm wavelength). The spectra were collected at a sampling rate of 250,000 spectra per second. The vertical axis in each plot is the digital value of the voltage on each of the phototransistors in the array. The maximum range is 0 to 255 (8-bit digital), corresponding to phototransistor voltages of zero to + 2.00 volts, respectively. In these spectra, the peak signal strength never exceeds a digital value of 40 (0.3125 mV). The horizontal axis is the phototransistor number in the array, from 1 (left point in each trace) to 32. Note the low-level noise present in spectrum **h**, which typically occurred in one out of every 6 spectra.

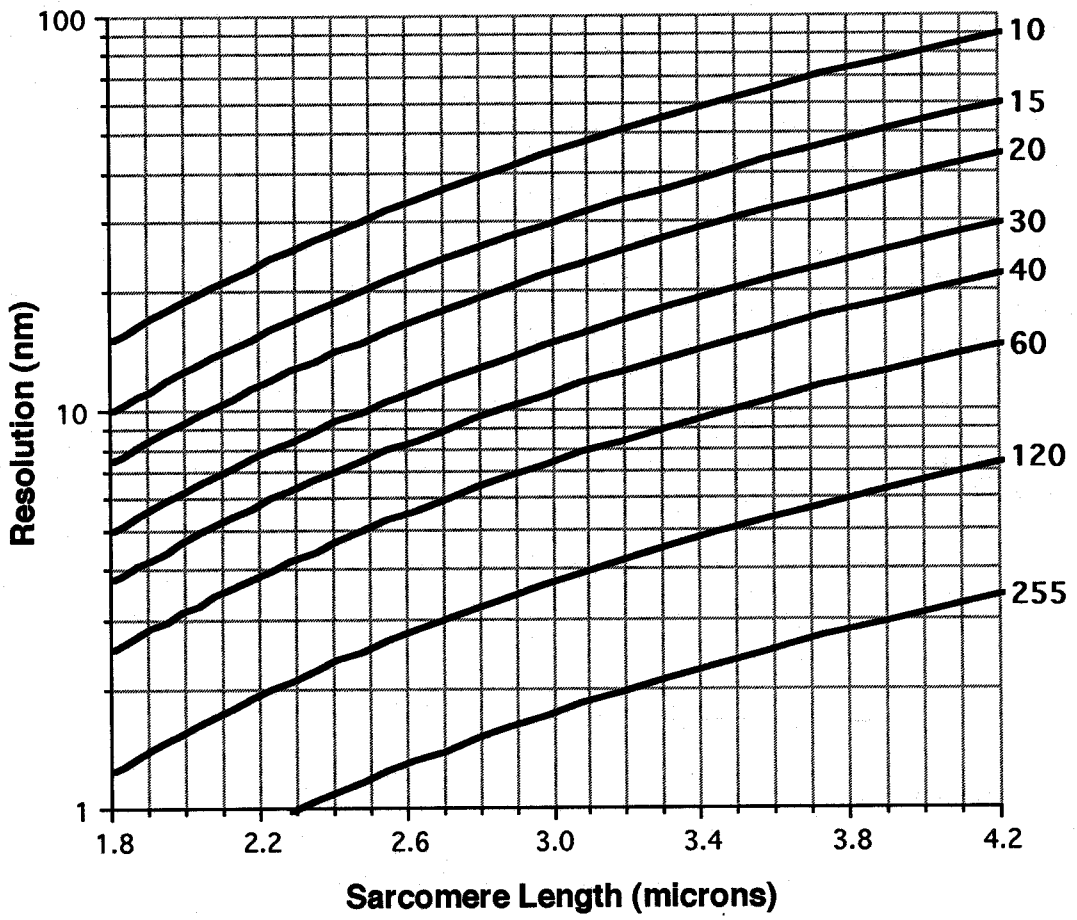

Figure 2.6. System resolution as a function of sarcomere length and peak digital signal strength. The vertical axis is the resolution in nanometers, the horizontal axis is the sarcomere length in microns. On the right hand side, each of the eight curves are labeled to indicate the peak digital signal strength of the first order diffraction spectrum. The maximum signal strength is 255, due to the 8-bit intensity resolution of the phototransistor array. The minimum acceptable peak value is 10. The resolution calculations assume the geometry used for this series of experiments, namely, a laser wavelength 632.8 nm, phototransistor width of 2.21 mm, phototransistor array tilt of 13.2 degrees, distance from fiber to phototransistor array of 290.5 mm, and distance from zero order peak to the center of diode #1 of 112 mm.

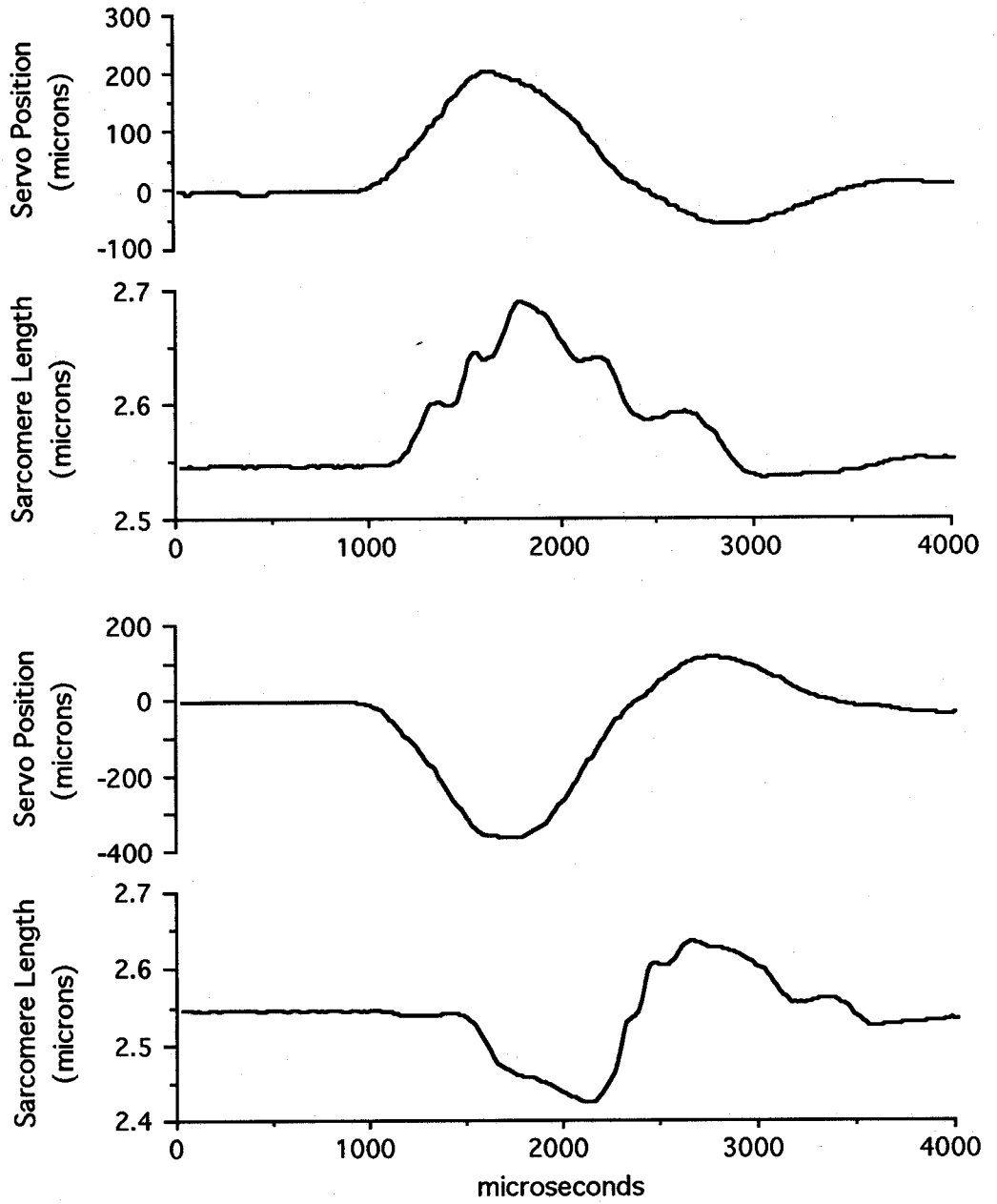

Figure 2.7. Typical data records from the single sinusoidal pulse propagation experiments. The data are from Fiber 19, battery 1. The top trace represents the servo position data during a lengthening pulse. Servo position is measured in microns from the neutral position. Note the slight overshoot after the single sinusoidal pulse. The trace directly below the top trace is the corresponding sarcomere length data from a point approximately 2 mm from the point at which the muscle fiber is attached to the servo. The bottom two traces are the servo position and the corresponding sarcomere length data for a large amplitude shortening pulse, sampled at the same position along the fiber as the top traces. These data are representative of the 14,592 pulses that were applied throughout this study. For all traces the fiber was fully relaxed. The fiber was from the soleus muscle of an F344 rat. The fiber length was 5.12 mm, at an initial sarcomere length of 2.55 microns/sarcomere.

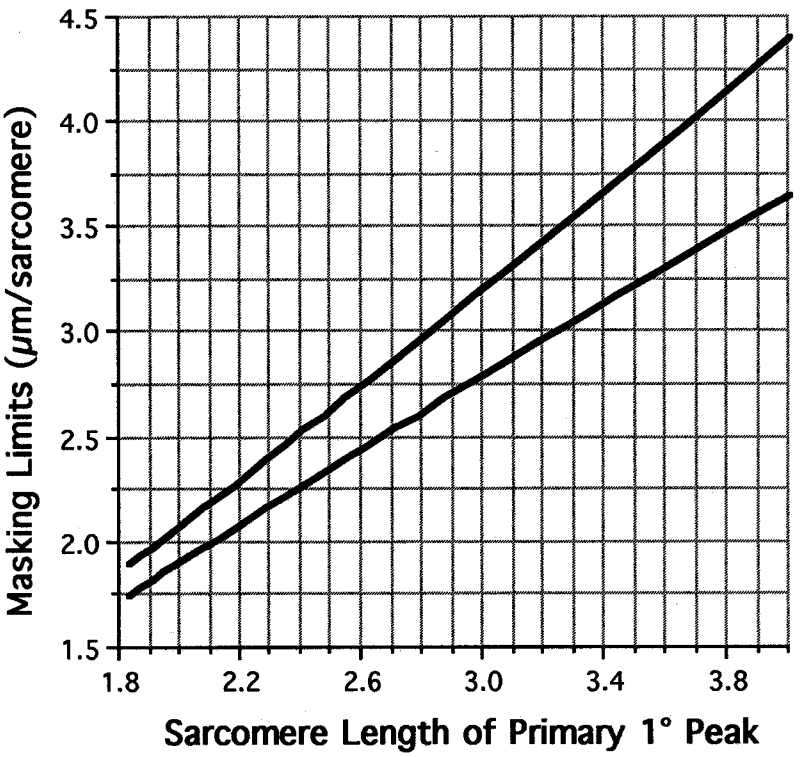

Figure 2.8. Masking of secondary peaks due to finite phototransistor size. If the area sampled by the laser spot on the muscle fiber contains areas with differing sarcomere lengths, the first order diffraction pattern will have multiple peaks (Judy, et al., 1982). The primary first order peak is defined as the peak with the greatest maximum signal strength. Lesser peaks are designated as the secondary, tertiary, and so forth. The spatial averaging of the first order diffraction peak signal that occurs because of the finite width of the phototransistors in the detector array limits the ability of the system to detect multiple peaks. This results in a masking of secondary and lesser peaks that do not differ from the primary peak by an amount sufficient to be detected by the array. The worst-case secondary peak masking range is shown in the graph. For a primary first order diffraction peak value that results in a calculated sarcomere length as shown on the abscissa, the system will not be able to detect a secondary or lesser peak for sarcomere lengths that fall within the range indicated on the ordinate by the two lines on the graph. This worst case description is based on the assumption of a minimum acceptable signal strength and a minimum peak separation of at least two phototransistor widths.

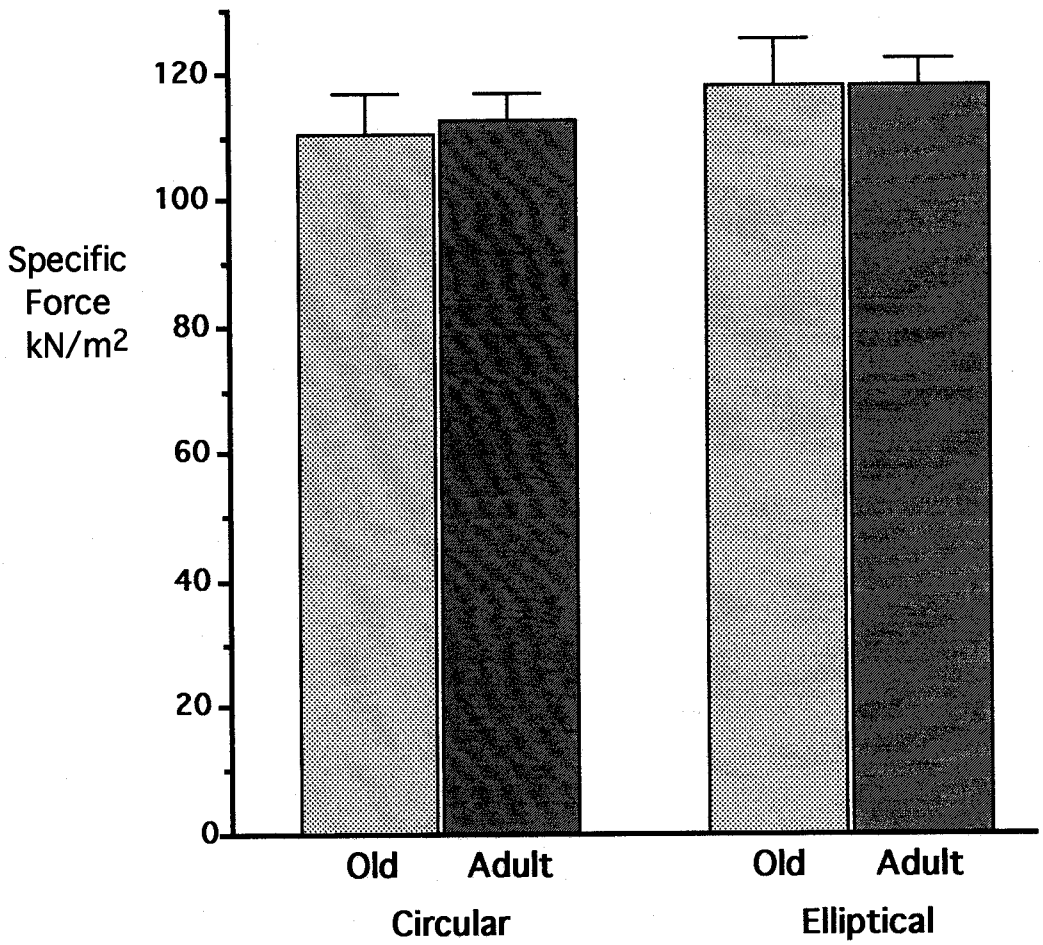

Figure 3.1. Specific force for single muscle fibers from adult (4 to 12 month) and old (27 month) F344 rats. There was no significant difference between the specific forces when the cross-sectional area was approximated as circular (left) or elliptical (right). The values shown are mean ± 1 SEM. For adult (4 to 12 month old) rats, the specific force was 112.3 ± 4.5 kPa (circular) and 117.7 ± 4.5 kPa (elliptical). For the old (27 month old) rats, the specific force was 110.2 ± 6.3 kPa (circular) and 118.0 ± 7.2 kPa (elliptical).

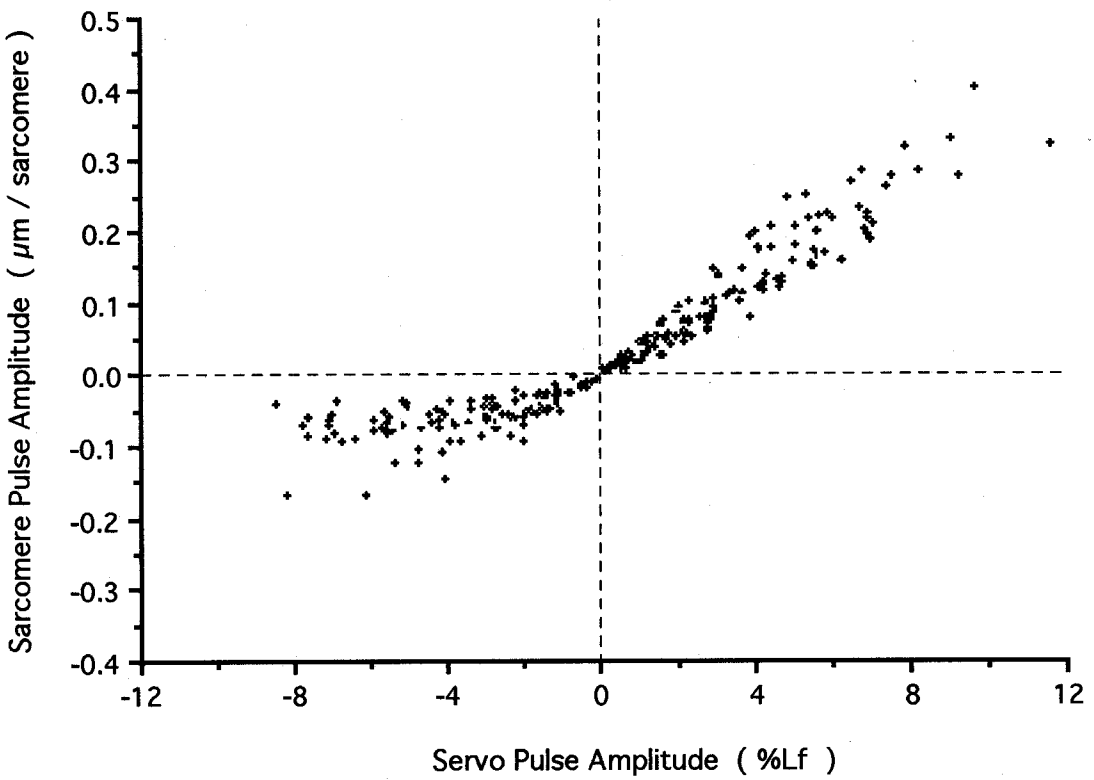

Figure 3.2. Fiber buckling during shortening pulses. Servo pulse amplitude (%Lf) is ploted on the abscissa, and the resulting sarcomere length pulse amplitude (μm/sarcomere) is plotted on the ordinate. The data are from all fibers when fully relaxed, at 1000 Hz pulse frequency. Note that, for a given absolute value of servo pulse amplitude, the resulting sarcomere length pulse amplitudes during shortening pulses (negative values) are less than those for lengthening pulses, indicating fiber buckling during shortening pulses.

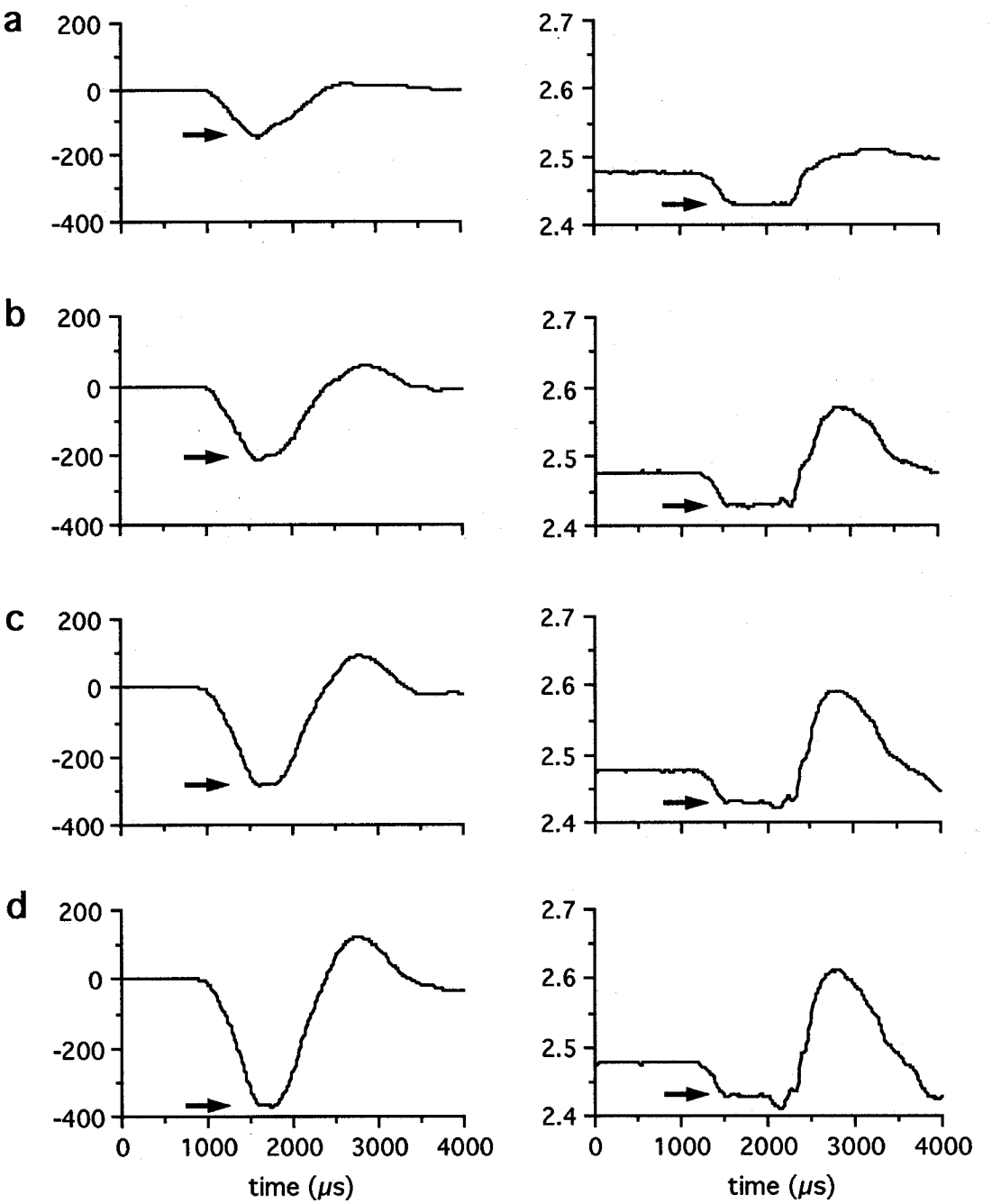

Figure 3.3. Evidence of muscle fiber buckling during shortening pulses of increasing amplitude. The data are from fiber 16. The fiber length was 7.10 mm. The fiber was fully relaxed and the shortening pulse frequency was 1000 Hz. The four plates on the left show the servo position data during each pulse, in microns from the neutral servo position. Each plate on the right shows the resulting sarcomere length data, in μm per sarcomere, from each of the four servo pulses. The abscissa for all plates is in units of μ sec. The sarcomere length data were measured 5.04 mm from the servo attachment point on the fiber. As the servo pulse shortening amplitude increases (from **a** to **d**), the resulting sarcomere length pulses plateau at approximately the same minimum, due to buckling of the fiber during shortening.

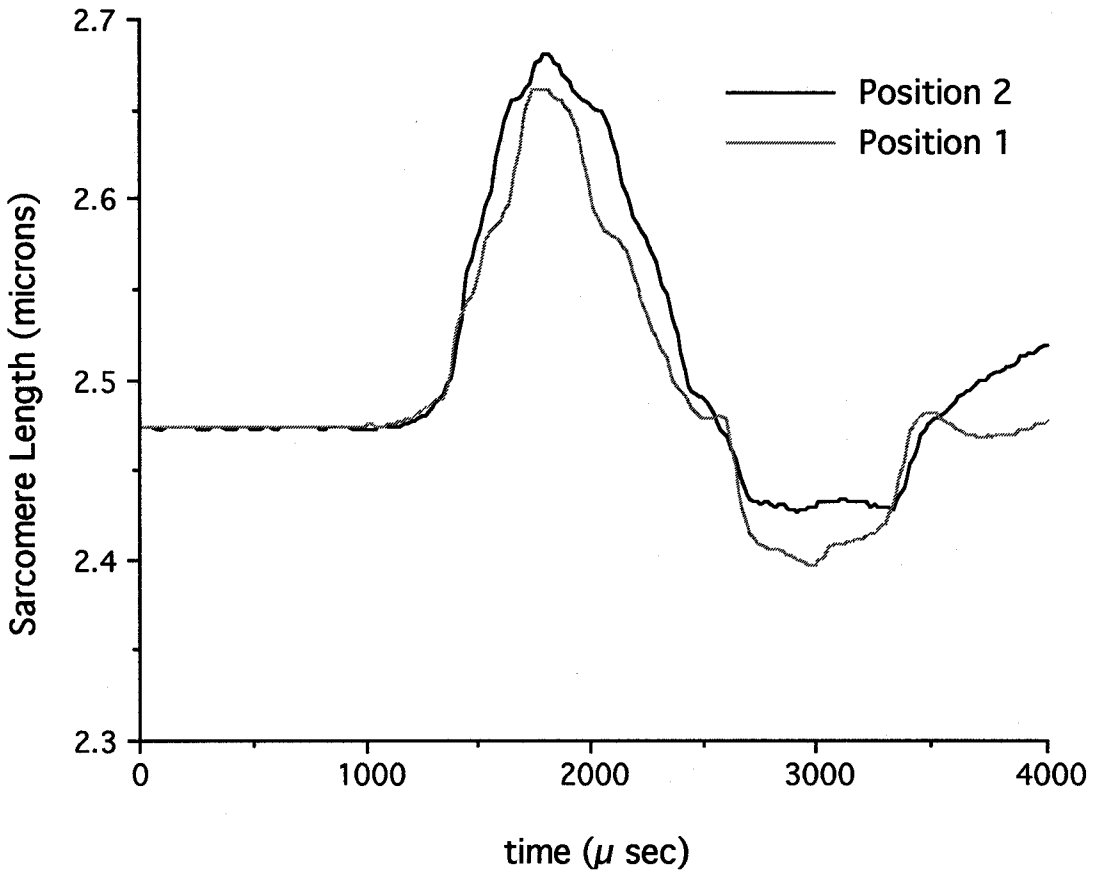

Figure 3.4. Strain pulse amplitude data for two sampling positions on fiber 16, separated by a distance of 1.34 mm. The fiber was 7.10 mm in length, was fully relaxed, and the lengthening pulse frequency was 1000 Hz. Data with minimal evidence of steps and pauses were selected for this figure to allow a visual comparison of the strain pulse amplitudes. The amplitude distortion due to the steps and pauses is generally much greater in the typical sarcomere length-time records. The data set contains 1024 time points for each trace. The pulse with slightly lower amplitude (gray) was recorded at position 1, which was 3.70 mm from the servo attachment point on the muscle fiber. The solid black trace was recorded at position 2, which was 5.04 mm from the servo attachment point. In both cases, the servo pulse amplitude was the same. This figure illustrates the fact that the strain pulse amplitude is distorted by the steps and pauses, even when the step and pause amplitude is minimal. Also, the strain pulse amplitude is apparently greater at position 2, which is further from the servo. The increased amplitude suggests negative damping of the strain pulse as it propagates along the fiber. In this case the difference in the strain pulse amplitudes is approximately 8%. In most of the sarcomere length-time records, the strain pulse amplitude difference is smaller than indicated in this figure.

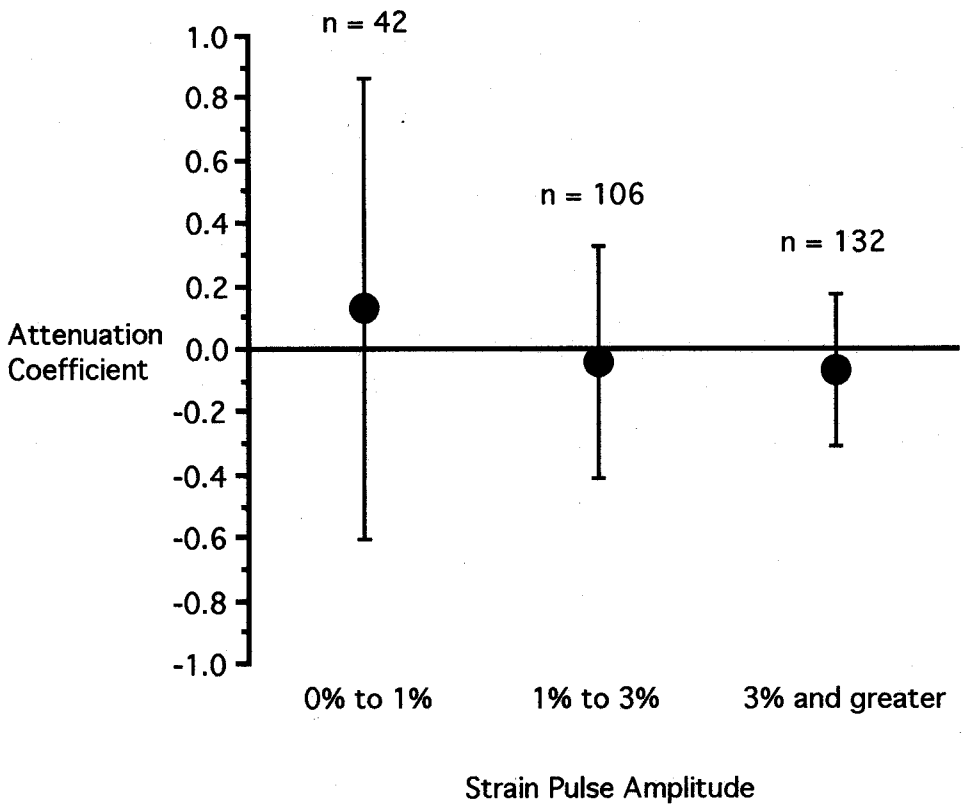

Figure 3.5. Average attenuation coefficients for lengthening pulses in fully relaxed fibers. Data are shown as mean ± std. dev. Attenuation coefficients for shortening pulses are not included because of buckling of fibers during shortening pulses. The data are for all fibers and include data from all pulse frequencies. Within each data set for each fiber, the data are grouped and averaged by pulse amplitude. Negative attenuation indicats that the sarcomere strain pulse amplitude increases as it propagates along the fiber. Attenuation coefficients for pulse amplitudes in the range of 0% to 1% and 1% to 3% are not significantly different from zero ($p > 0.05$). For pulse amplitudes greater than 3%, the attenuation coefficient is significantly different from zero ($p < 0.05$).

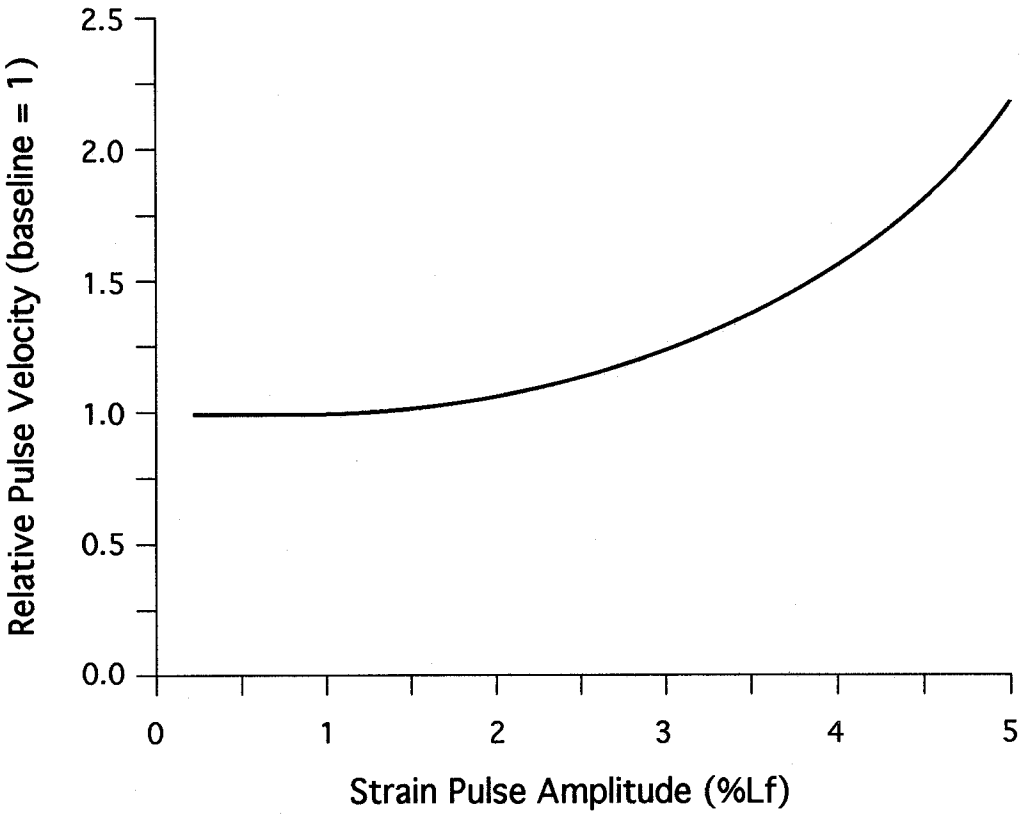

Figure 3.6. Schematic representation of the expected non-linear relationship between pulse propagation velocity and strain pulse amplitude, based on the published data for single muscle fiber stiffness as a function of increasing sarcomere length for relaxed mammalian muscle fibers. The data are based on Granzier and Wang, 1993b, Fig. 8b. The relationship assumes a baseline sarcomere length of 2.5 μm per sarcomere. The elastic modulus is proportional to the square of the pulse propagation velocity, if the pulse is propagated with negligable attenuation. Thus, for strain pulse amplitudes of approximately 5%, the stiffness was expected to be approximately four times greater than the baseline stiffness at very low strain pulse amplitudes.

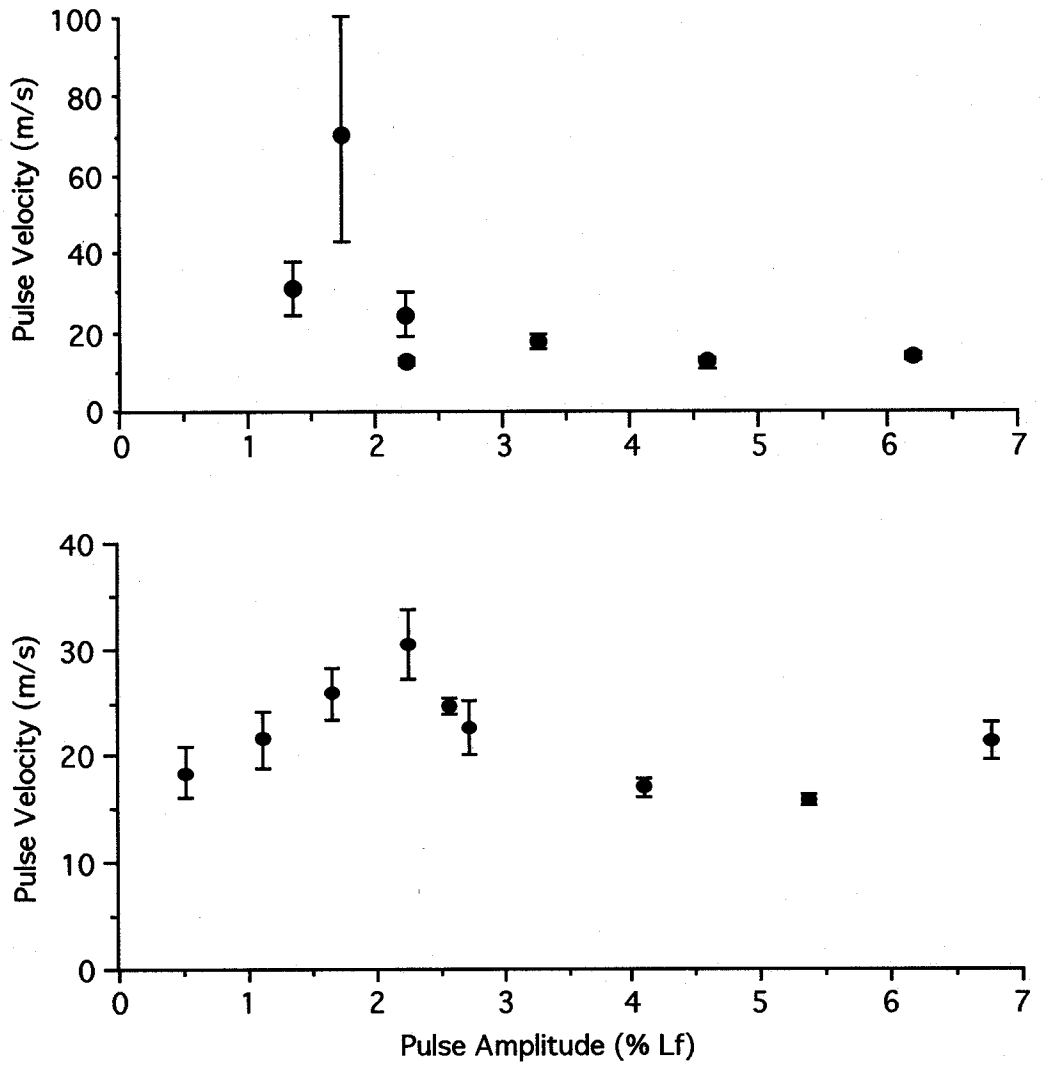

Figure 3.7. Evidence of the effect of pulse amplitude on pulse propagation velocity. Each data point represents the average of 6 or 7 pulses, ± 1 standard error. The top trace is from fiber 6; the baseline sarcomere length is 2.58 μm and the 1 kHz lengthening pulses were applied while the fiber was fully relaxed. The bottom trace is from fiber 21; the baseline sarcomere length is 2.55 μm and the 1 kHz pulses were applied while the fiber was fully relaxed. Note the peak pulse propagation velocity, which typically occurs at pulse amplitudes between 1% and 4% Lf for most of the fibers. Most of the data sets were not as complete as those shown above. Several of the data sets had pulse propagations that were too fast to be measured accurately (above 125 m/s), and in every case these occured in the 1% to 4% Lf range.

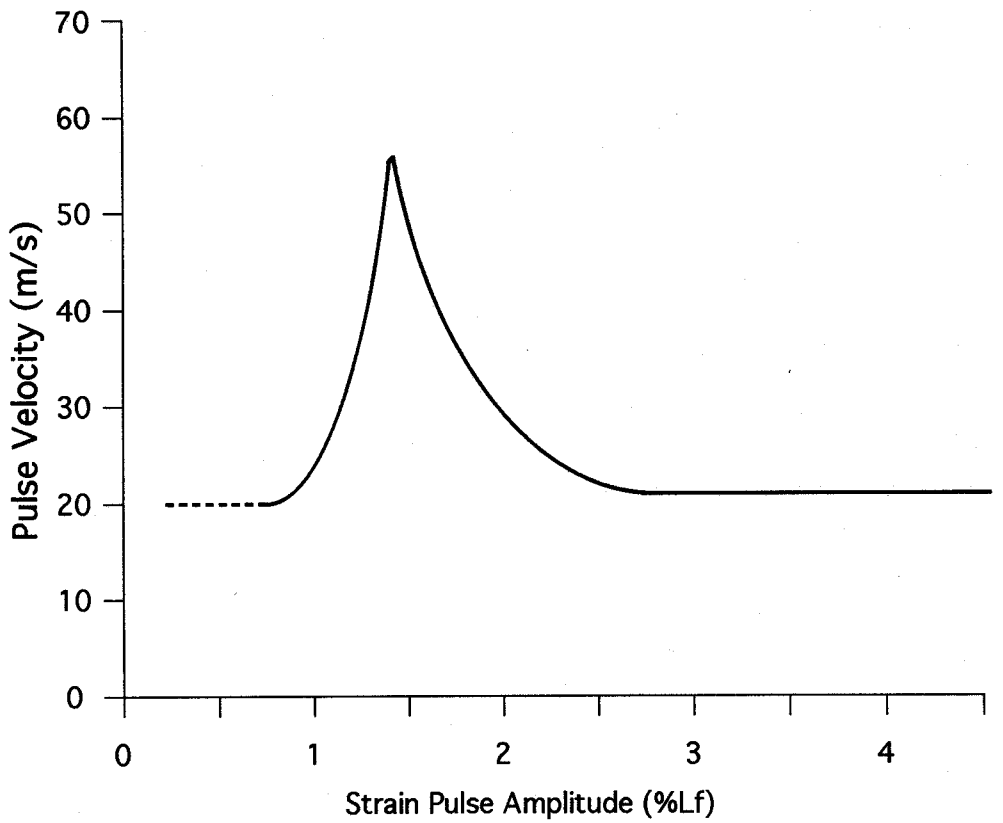

Figure 3.8. Schematic representation of the proposed recoverable yield, illustrated in terms of pulse propagation velocity as a function of strain pulse amplitude. The elastic modulus is proportional to the square of the pulse propagation velocity, if the pulse is propagated with negligable attenuation. Values for the pulse propagation velocity baseline and peak, and the location of the recoverable yield point are arbitrary, but are based on average values from the representative data set.

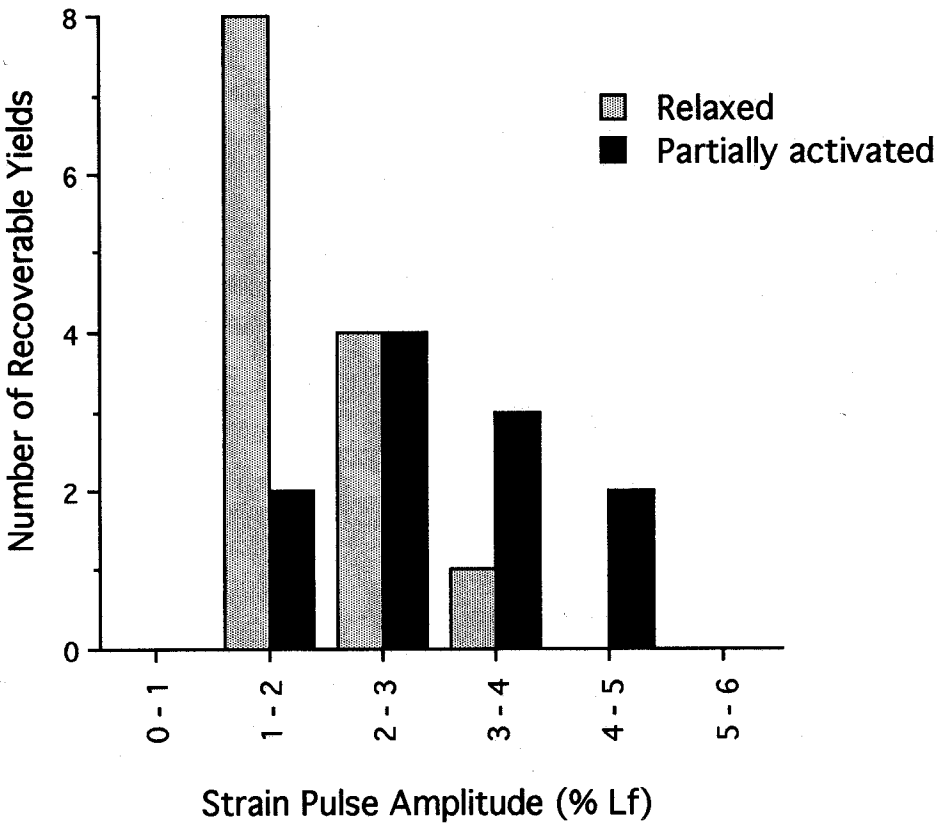

Figure 3.9. Distrubution of the non-linear peaks as a function of strain pulse amplitude, for relaxed fibers and partially activated fibers. Of the total 19 fibers in this study, 15 had sufficient data throughout the range of strain pulse amplitudes to detect non-linear behavior in the range of 1% to 5% Lf. Eleven of the 15 fibers exibited clear non-linear peaks for some value of strain pulse amplitude. The non-linear peaks occur at larger strain pulse amplitudes for partially activated fibers than for fully relaxed fibers. The figure includes data for strain pulse frequencies in the range of 500 to 2000 Hz. The partially activated fibers include data for fibers at 3% to 34% activation.

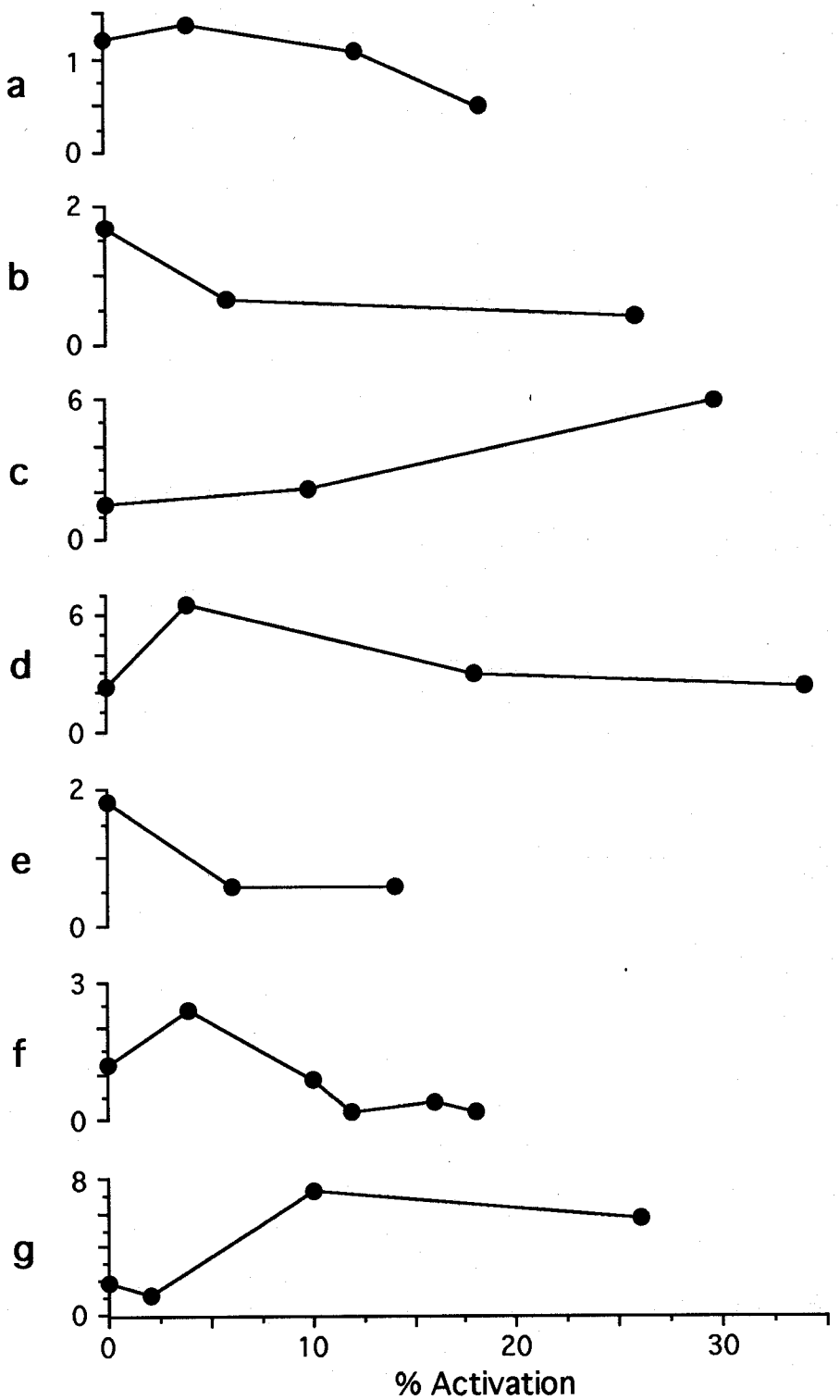

Figure 3.10. Elastic modulus as a function of percent activation for fibers at low levels of activation and full relaxation. Elastic modulus was calculated for 1000 Hz lengthening pulses in the amplitude range of 4% to 8% Lf. The ordinate for each plate is in units of MPa. The data are: (a) fiber 4, (b) fiber 5, (c) fiber 9, (d) fiber 10, (e) fiber 14, (f) fiber 15, (g) fiber 16.

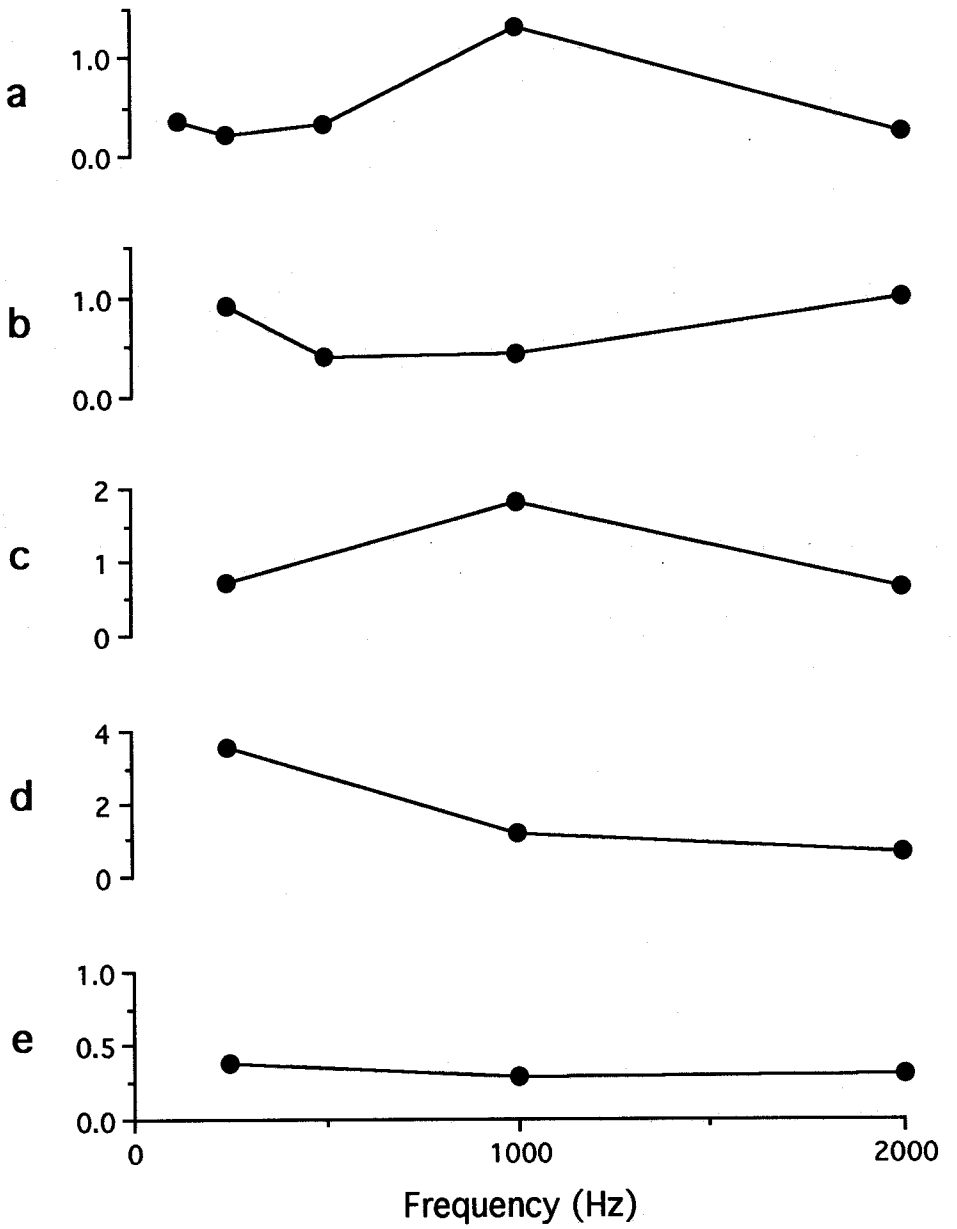

Figure 3.11. Elastic modulus as a function of frequency for fully relaxed fibers. The ordinate for each plate is in units of MPa. The data are from: (a) fiber 6, (b) fiber 7, (c) fiber 14, (d) fiber 15, (e) fiber 18. These data illustrate the fact that, although all of the elastic modulii are of the same order of magnitude for fully relaxed fibers, there is no relationship between elastic modulus and pulse frequency for the range of frequencies used. This may result from the fact that the pulse amplitudes are very large, in the range of 4% to 8% Lf, to avoid the range of non-linear behavior in each data set for each fiber.

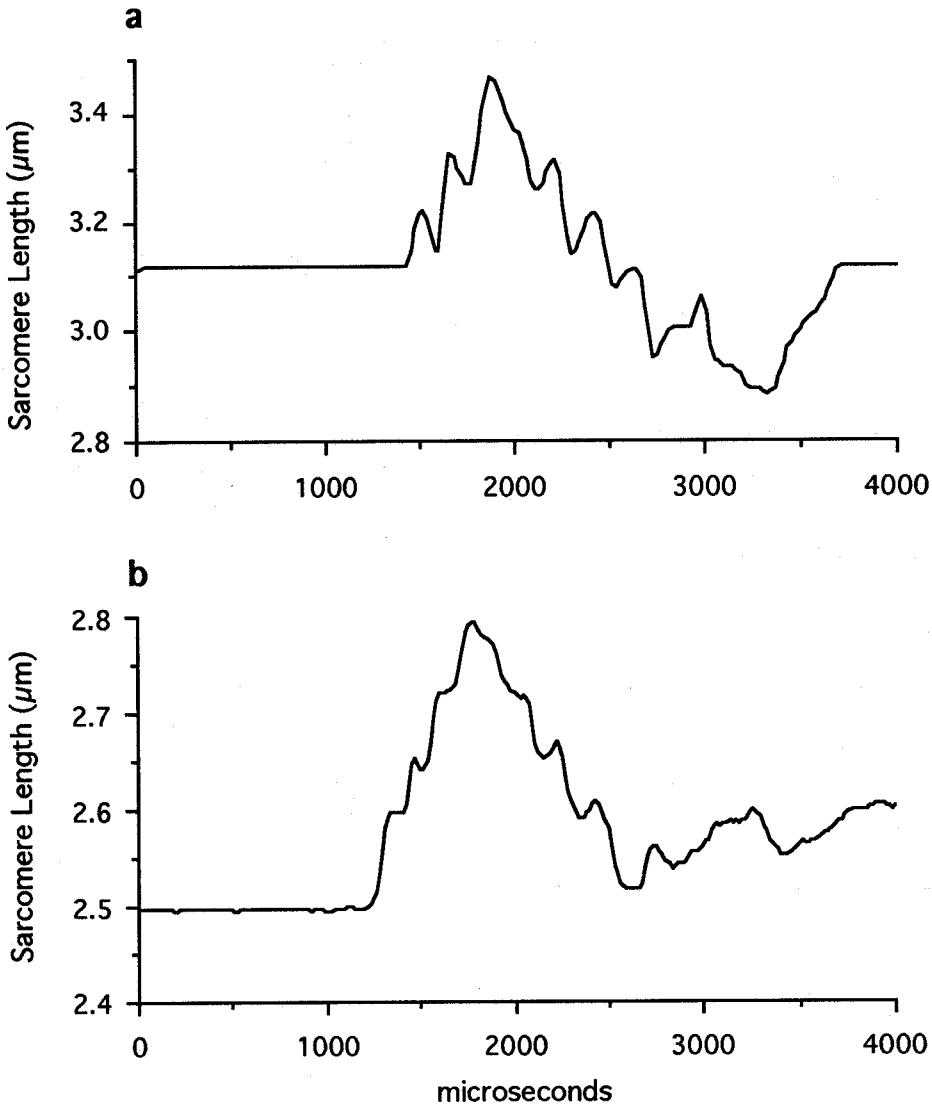

Figure 4.1. Typical sarcomere length vs. time records for lengthening strain pulses. These traces were selected at random and are representative of approximately 7000 lengthening pulses applied to 21 different muscle fibers while sampling with a He-Ne laser focused to a 250 micron diameter spot. The top trace (**a**) is from fiber #4, battery 8, pulse #109. The bottom trace (**b**) is from fiber #7, battery 1, pulse #54. Both fibers were from the soleus muscle of F344 rats. In both cases, the fibers were fully relaxed and maintained at 15 °C. The single sinusoidal pulse frequency was 1 kHz in both cases also. Note that the baseline sarcomere length is approximately 3.1 microns in trace **a**, whereas it is approximately 2.5 microns in trace **b**. Steps such as these were evident for all lengthening pulses at all pulse amplitudes and frequencies, and at all levels of activation when a He-Ne laser was used as the light source.

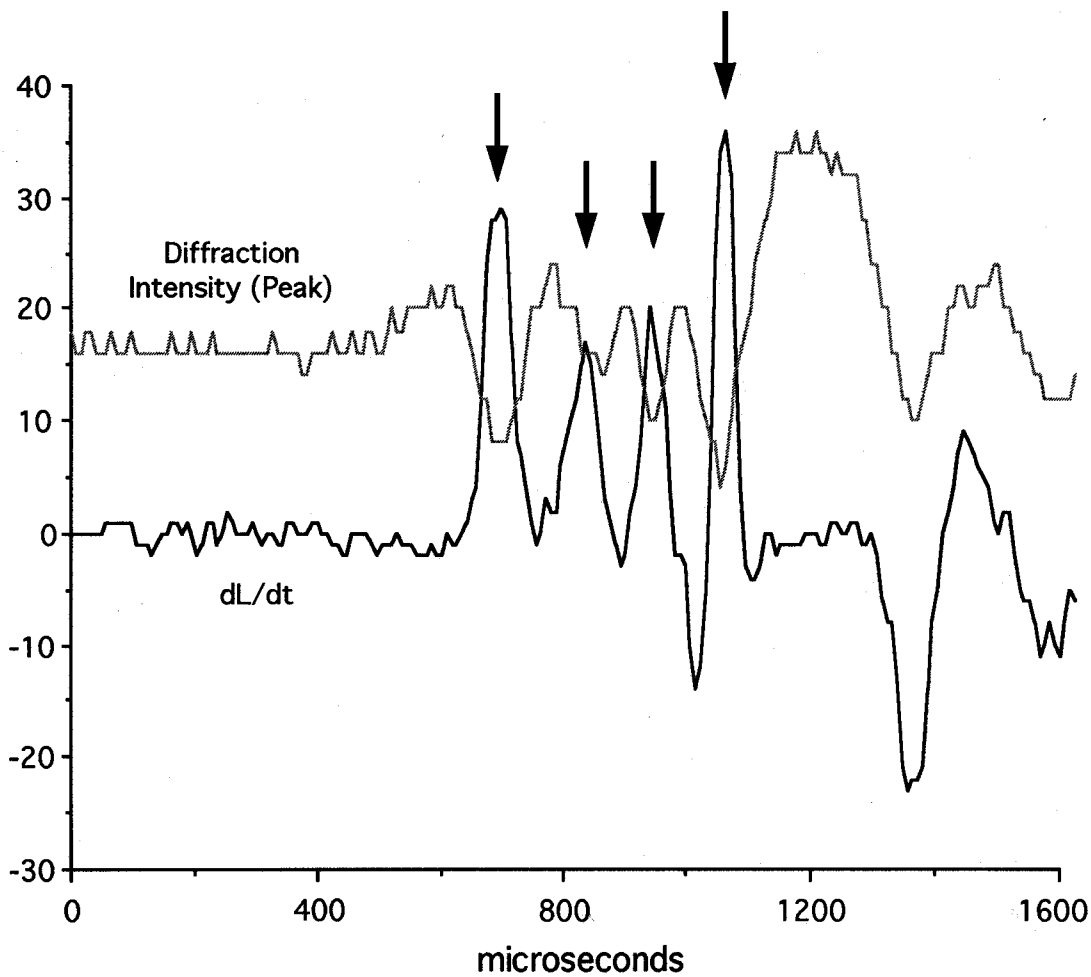

Figure 4.2. Correlation between rate of change of sarcomere length (dL/dt) and 1° diffraction peak intensity. The top trace (dotted line) indicates the peak intensity of the 1° diffraction peak for a lengthening pulse (Fiber #21, battery 1, pulse #5). The fiber is fully relaxed. The ordinate is in units of 8-bit digital signal strength for the first order peak intensity trace, and units of microns per sarcomere per sampling interval for the rate of change of sarcomere length. Thus, for the diffraction intensity, the units represent discrete intensity levels of the diffraction peak, with a maximum value of 255 and a minimum value of 0. The time scale is truncated to focus on the initial portion of the sarcomere length pulse. Note that four steps occur (indicated by the arrows) as the sarcomere length increases to the peak value, which occurs around 1200 microseconds. The maximum rate of change of sarcomere length (the steepest part of each step on the sarcomere length vs time records) is always closely corelated with a drop in diffraction peak intensity. This figure is representative of 24 pulse data records which were chosen at random. In all cases the minimum first order diffraction peak intensity corresponds with the maximum positive slew rate of each of the sarcomere length steps in each sarcomere length vs time record. These results are identical to those of Burton and Huxley (1995) for slow lengthening and shortening ramps.

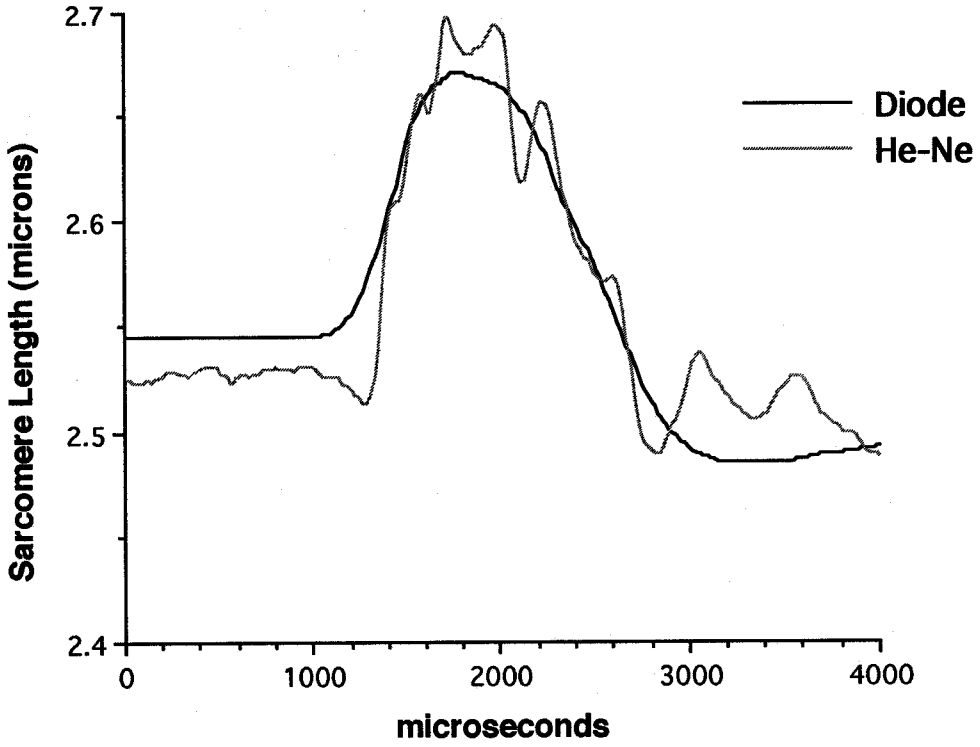

Figure 4.3. Elimination of steps and pauses by the use of a laser of short coherence length. The data is from fiber # 22, a relaxed soleus muscle fiber from the rat. Initially, the fiber was subjected to a full battery of 128 lengthening and shortening pulses with 1 kHz single sinusoidal length pulses. A Helium Neon (He-Ne) laser was focused to a diameter of 250 microns, near the center of the fiber, and the resulting diffraction pattern was collected. The resulting sarcomere length vs. time trace for one of the representative lengthening pulses is shown in grey. The He-Ne laser was replaced with a diode laser module, powered at + 4.90 volts to minimize the coherence length, as described in the text. The fiber was then subjected to the same battery of 128 lengthening and shortening pulses while fully relaxed. A representative trace for sarcomere length vs. time is shown in solid black. Note that the steps and pauses, which are clearly evident in the trace in which a He-Ne laser is used, are entirely absent when a diode laser is used. These data are representative of data from 21 fibers subjected to a total of nearly 15,000 pulses with a He-Ne light source. All data from fibers sampled with a He-Ne laser show evidence of steps and pauses, whereas, for three fibers, subjected to a total of 768 pulses with a short coherence-length laser diode as the light source, no steps or pauses were evident.